2021 43rd Annual International Conference of the
IEEE Engineering in Medicine & Biology Society (EMBC)
Oct 31 - Nov 4, 2021. Virtual Conference

Estimating Human Upper Limb Impedance Parameters From a State-of-the-Art Computational Neuromusculoskeletal Model

Morteza Asgari, Dustin L. Crouch, *Member, IEEE*

***Abstract*—The human neuro-musculoskeletal system constantly deploys passive (e.g., posture adjustment) and active (e.g., muscle co-contraction) control strategies to regulate upper limb impedance and stability while interacting with the outside world. Upper limb impedance has been assessed through *in vivo* experiments and model-based simulations. The experiments are practically limited to small samples of able-bodied subjects and few limb postures, and model-based approaches have mostly used simplified upper limb models. Our objective was to develop and validate a computational approach to estimate upper limb impedance parameters - stiffness, viscosity, and inertia - at the endpoint (i.e., hand) using a neuromusculoskeletal model with realistic geometry. We added a planar manipulandum to an existing upper limb model implemented in OpenSim (version 3.3) and used contact modeling to attach the manipulandum's handle to the musculoskeletal model's hand. The hand was placed at several locations lateral to the shoulder joint along anterior/posterior and medial/lateral axes. At each location, during forward dynamics simulations, the manipulandum applied small perturbations to the hand in eight different directions. The spatial variation of the computed, model-based impedance parameters was similar to that of experimentally measured impedance parameters. However, the overall size of the stiffness and viscosity components was larger in the model than from experiments.**

***Clinical Relevance*— Computational modeling and simulations can estimate upper limb impedance properties to complement and overcome the limitations of experiments, especially for clinical populations. The computational approach could ultimately inform new interventions and devices to restore limb stability in people with shoulder disabilities.**

I. Introduction

The mechanical impedance of the human upper limb describes the limb's ability to resist moving when it is displaced from an equilibrium position [1], [2]. It is well-established that the human neuro-musculoskeletal system regulates limb impedance both passively (e.g., posture) and actively (e.g., muscle contraction) to maintain stability while manipulating objects and interacting with the environment [3]. There are many common orthopedic (e.g., rotator cuff tear) [4] or neurological (e.g., stroke) injuries that often lead to devastating shoulder disability. There is evidence that such disability can impair the passive and active mechanisms of the neuro-musculoskeletal system for impedance modulation, destabilizing the shoulder joint and hand position [5].

Impedance can be characterized by physical parameters stiffness, viscosity, and inertia from engineering dynamics [2]. The stiffness and viscosity components originate from properties of the musculoskeletal system's passive and active tissues and can be further regulated by changing levels of muscle activation and co-activation. However, the inertia only depends on the posture and physical properties of the upper limb, like mass and length [6]. The standard technique to identify the impedance parameters is to build a second-order linear model from the experimental hand force field data [6], [7]. The hand force field describes the relation between displacements and restoring forces when the hand is perturbed about a given equilibrium position. Perturbations are typically applied to the hand by a planar robotic manipulandum. Impedance can be estimated either at the endpoint (i.e., hand) or at the joint level (i.e. shoulder and elbow) [3].

Impedance has been either measured experimentally or estimated computationally. Due to practical reasons, experimental studies have limited testing to small numbers of able-bodied subjects (due to risk of injury to people with disability), trials (due to subject fatigue), and limb postures. At the same time, model-based studies have mainly used simplified models (e.g. with less muscles than the biological limb) [8] or only estimated the stiffness parameter using muscle short-range stiffness modeling [9]. These limitations prevent full understanding of how the neuromusculoskeletal system regulates impedance over the entire upper limb workspace under healthy and impaired conditions. Addressing this knowledge gap would inform new interventions and devices to help regulate impedance and restore limb stability in people with shoulder disability.

Computational approaches and simulations with more realistic musculoskeletal models can complement and overcome the limitations of previous studies to more fully characterize the impedance properties of the upper limb. Thus, the overall objective of the proposed project was to develop a computational approach using an upper limb neuromusculoskeletal model with realistic geometry to estimate upper limb impedance parameters and validate the computational impedance results against published experimental results.

II. Methods

A. Modelling the musculoskeletal-manipulandum system

Our strategy in this preliminary study was to replicate a typical experiment set-up [6]. We added a planar two-joint manipulandum to an existing upper limb musculoskeletal model [10] implemented in OpenSim (version 3.3) [11]. The

*Research supported by the University of Tennessee, Department of Mechanical, Aerospace, and Biomedical Engineering.

M. Asgari is with the Department of Mechanical, Aerospace, and Biomedical Engineering, University of Tennessee, Knoxville, TN 37996 USA (e-mail: morteza_asgari@ utk.edu).

D. L. Crouch is with the Department of Mechanical, Aerospace, and Biomedical Engineering University of Tennessee, Knoxville, TN 37996 USA (phone: 865-974-7656 e-mail: dustin.crouch@utk.edu).

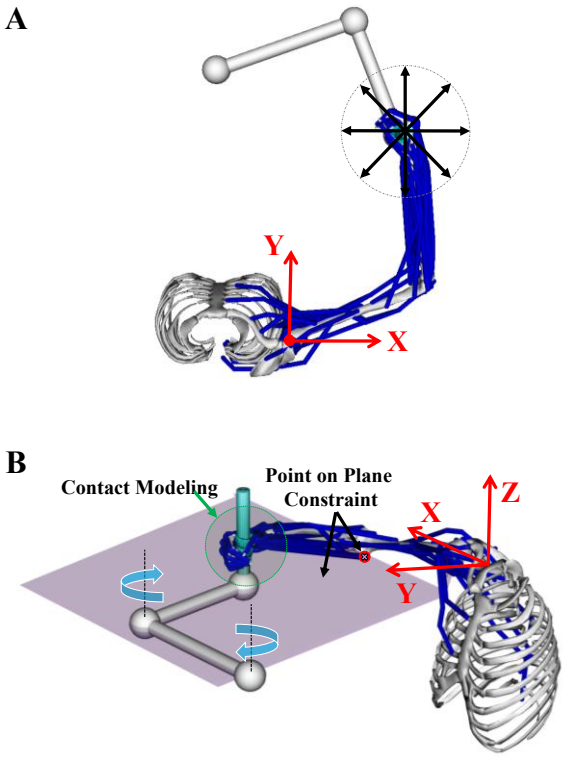

Figure 1. Musculoskeletal-manipulandum model. A) The arrows show the eight directions of perturbations applied to the hand. B) The meshed geometry of the handle was surrounded with three meshed disc geometries to represent the hand grip. The humerus trochlea was constrained to move on the horizontal plane.

upper extremity model had 7 degrees of freedom, with three describing the shoulder kinematics and four describing the elbow and wrist kinematics. The model geometry is defined based on a 50th percentile male population's anthropometric data and contains fifty Hill-type muscle-tendon units crossing shoulder, elbow, and wrist joints. The manipulandum consisted of two rigid cylindrical links and massless torque actuators. The links have lengths of 0.30 and 0.25 m and moments of inertia of 0.0037 and 0.0013 $Kg.m^2$, respectively. The inertia of the manipulandum (i.e., mass matrix) was designed to be smaller than the upper limb to minimize the effect of nonlinear dynamic forces on simulated movements. The torque actuators were placed at the manipulandum joints to apply torques about the *z-axis* in the global coordinate system (Fig. 1). The manipulandum included a handle (i.e., end-effector) whose centroid point along the *z-axis* was aligned with the shoulder along the *z-axis*.

We used contact modeling to attach the handle to the model's hand using OpenSim's elastic foundation algorithm. To resemble the fingers' grip around the handle, the meshed geometry of the handle was placed inside three meshed disk geometries. Contact parameters of stiffness and dissipation were set, respectively, to 25x10^6 (N/m) and 0.4 Ns/m. Other coefficients of static, dynamic, and viscous friction were also defined based on Savescu's work [12].

A linear PD controller placed the handle in any desired position across the limb's reachable workspace and applied external perturbations to the hand (Fig. 1(A)). We used the following control law to determine the torque vector required to navigate the handle position:

$$\tau = J(q)^T\left[K_m(X_d - X) - B_m\dot{X}\right] \quad (1)$$

where τ is the torque vector; $J(q)$ is the Jacobian matrix defining the handle cartesian displacement from the manipulandum joint angles q; K_m and B_m represent the manipulandum stiffness and viscosity matrices, respectively; X_d is the desired position; X and $\dot{X}$ show the current position and velocity vectors of the handle. In this study, we fine-tuned the stiffness and viscosity matrices as:

$$K_m = \begin{bmatrix} 400g & 0 \\ 0 & 400g \end{bmatrix}(N/m),\ B_m = \begin{bmatrix} 150g & 0 \\ 0 & 150g \end{bmatrix}(Ns/m)$$

where g is the gravitational constant.

B. Forward dynamics

Though the upper limb was supported against gravity during experiments, participants may have had to actively hold their upper limb in the desired static posture while holding the manipulandum's handle. Thus, we used computed muscle control (CMC) to compute the steady-state muscle excitations required to hold the upper limb in a static posture at each of the handle's starting points. During CMC, the gravity field was set to zero. We assumed that changes in muscle excitations caused by the small hand perturbations during the experiment were negligible; thus, the steady-state muscle excitations were applied to the respective muscles at corresponding handle starting points throughout forward dynamics simulations.

At the start of each forward dynamics simulation, the manipulandum's handle (with hand attached) was moved to the starting point using the feedback control law (Eq. 1). Given the model's limited workspace in which muscle-tendon moment arms were previously validated [10], we chose starting points that were lateral to the shoulder joint. Eight equally spaced starting points (5 *cm* apart) were 33 *cm* anterior to the shoulder joint and from 3 to 48 *cm* along the *x-axis* (medial/lateral direction). Another eight equally spaced starting points were 23 *cm* lateral to the shoulder and from 13 to 48 *cm* along the *y-axis* (anterior/posterior).

Once at the starting point, the manipulandum perturbed the hand in eight different directions. To ensure that the model's hand and manipulandum handle were at rest, perturbations were applied first at 3 s after reaching the starting point then every *0.6* s thereafter. During perturbations, the wrist joint

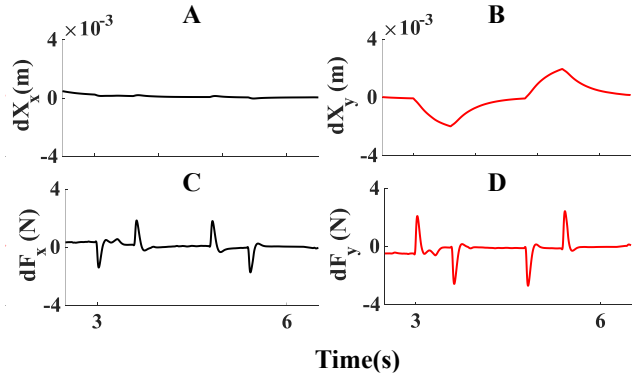

Figure 2. Sample handle displacements in *x* (A) and *y* directions (B) with corresponding restoring forces in *x* (C) and *y* directions (D) for a perturbation in *y-axis*.

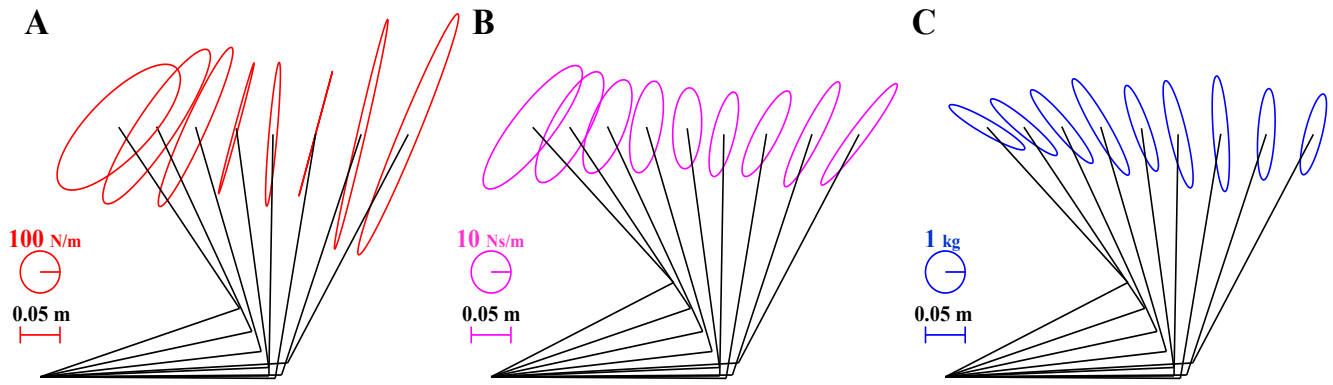

Figure 3. Estimated Stiffness (A), Viscosity (B), and Inertia ellipses (C) when hand displaced in the medial/lateral direction.

movement was limited by a rotational bushing force to mimic typical bracing used in experiments. Since participants' upper limbs were supported against gravity during experiments, the movement of the distal point of the humerus was constrained to only move in the horizontal plane at shoulder level (Fig. 1(B)) and the gravitational acceleration was set to zero. We set the perturbation amplitude and duration to 2 *mm* and 1.2 *s*, respectively. Handle displacements and restoring forces (i.e., contact forces) were recorded during simulations.

C. Upper limb endpoint stiffness estimation

To estimate the hand impedance parameters, we regressed a second-order linear model (Eq. 2) to the simulated force field similar to the earlier studies [5, 6].

$$\boldsymbol{M}d\ddot{X}(t) + \boldsymbol{B}d\dot{X}(t) + \boldsymbol{K}dX(t) = -dF(t) \qquad (2)$$

where $\boldsymbol{M}$, $\boldsymbol{B}$, and $\boldsymbol{K}$ are inertial, viscosity, and stiffness matrices of the hand impedance, respectively; $d\ddot{X}(t)$, $d\dot{X}(t)$, and $dX(t)$ display, in order, the change in vectors of acceleration, velocity, and displacement of the handle, and $dF(t)$ is the change in restoring forces from perturbation onset. Handle acceleration and velocity were computed by taking second- and first-order derivatives from displacements. We wrote the impedance matrices of $\boldsymbol{M}$, $\boldsymbol{B}$, and $\boldsymbol{K}$ as the sum of a symmetric and an antisymmetric matrix. The symmetric and antisymmetric components define, respectively, the conservative and non-conservative parts of the hand force field (i.e., the relation of hand restoring forces to displacements). We visualized the conservative force field with graphical ellipses whose size, principal semi-axes (i.e., shape), and orientation are defined based on the determinant, eigenvalues, and eigenvectors of the symmetric impedance matrices, respectively. Each ellipse depicts the locus of restoring forces for hand perturbations in every direction by order of one unit (e.g., *1 m* displacement for the stiffness). Thus, ellipses with a larger area (i.e., size) represent higher restoring forces at limb posture, and the ellipse's major and minor axes determine the values and directions of the highest and lowest restoring forces, respectively.

III. Results and Discussion

Fig. 2 shows the typical handle displacements and restoring forces for perturbations along the *y-axis* from one starting point. Figs. 3 and 4 represent the ellipses of the estimated hand stiffness, viscosity, and inertia for starting points along the medial/lateral and anterior/posterior directions, respectively. At more medial and posterior starting points, the stiffness ellipses had lower eccentricity (Fig. 3(A), 4(A)) and the major axis orientation (i.e., high stiffness direction) changed towards the shoulder joint. For more extreme hand positions, the stiffness ellipses were mainly elongated in the major axis direction, but for medial/posterior

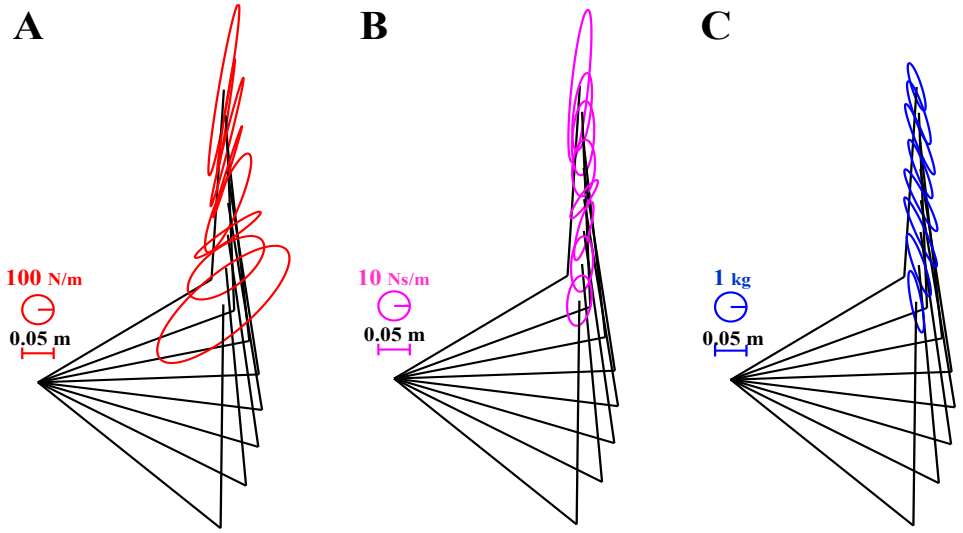

Figure 4. Estimated stiffness (A), Viscosity (B), and Inertia ellipses (C) for lateral hand positions when moved in the anterior/posterior direction.

positions, the stiffness ellipses became wider. This confirmed that hand restoring forces were higher and more isotropic for postures that are more central and proximal to the shoulder joint, consistent with results from Tsuji [6] and Mussa-Ivaldi [1]. However, the overall size of our stiffness ellipses is larger than the values reported in [6] but smaller than the ones reported in [1]. The observed spatial pattern for stiffness ellipses is most likely due to increasing passive forces of biarticular muscles (e.g., triceps long head) and higher muscles activation at higher elbow flexion and shoulder horizontal adduction angles.

The spatial pattern of the viscosity ellipses was similar to that of the stiffness ellipses, consistent with experimental results [6], [7]. The major axis of viscosity was aligned more towards the shoulder joint (Fig. 3(B), 4(B)), reflecting that the largest restoring forces against the speed occurred in the radial direction of the shoulder joint. The eccentricity of viscosity ellipses decreased toward more medial and posterior starting points, consistent with experiments [6]. The size of our viscosity ellipses, however, was substantially larger compared to experimental results. We suspect that viscosity is likely most influenced by muscles force-velocity relationships, muscles damping ratios, and hand-handle interaction.

The shape and orientation of the estimated inertia ellipses were well-matched with the experimental results. It is expected that the major axis of inertia ellipses will be nearly parallel with the distal segment of the limb (i.e., forearm/hand). This spatial pattern can be seen in Fig. 3(C) and 4(C) where the inertia ellipses rotated with the forearm/hand segment. To assess whether the estimated inertia ellipses were reasonable, we compared them to inertia ellipses computed for a two-joint arm whose links were cylindrical and have the same lengths and masses as the model's upper arm and forearm/hand. Compared to the calculated inertia ellipses, the estimated ones had similar orientations and shapes but smaller eccentricity and size (Fig. 5). From these observations, we can infer that our modeling approach under-estimated the restoring forces against the acceleration.

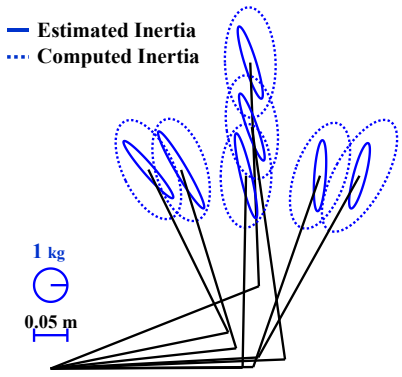

Figure 5. Estimated inertia from simulation vs. computed inertia from a simplified arm model with similar masses and lengths to that of the model's arm.

CMC does result in co-contraction of agonist-antagonist muscle pairs, but only to the minimum extent required to perform a simulated movement. Humans may vary the amount of co-contraction depending on other task goals (e.g., postural stability). Thus, future studies should explore the effect of co-contraction level on upper limb impedance.

I. Future Work & Conclusion

Our preliminary results suggest that computational modeling and simulation can estimate upper limb impedance properties to complement and overcome the limitations of previous experimental and computational studies. Our simulation-based results were fairly consistent with experimental results as: 1) the orientation of the stiffness and viscosity ellipses were toward the center of glenohumeral joint; 2) the eccentricity of the stiffness and viscosity ellipses increased toward anterior and lateral extreme hand positions; 3) the inertia ellipses were nearly parallel to the forearm/hand segment. There were, however, differences in the sizes of the inertia and viscosity ellipses between our model and previous experiments. These differences may be due to differences in muscle co-contractions and stretch reflexes between humans and the model, oversimplification of muscles and ligaments in the model, and missing passive human body components such as skin, veins, and cartilage. In future studies we will (1) refine the computational approach to predict experimental data more accurately and (2) identify how anatomical and biomechanical features influence upper limb impedance.

References

[1] F. A. Mussa-Ivaldi, N. Hogan, and E. Bizzi, "Neural, mechanical, and geometric factors subserving arm posture in humans," *Journal of neuroscience,* vol. 5, no. 10, pp. 2732-2743, 1985.

[2] J. M. Dolan, M. B. Friedman, and M. L. Nagurka, "Dynamic and loaded impedance components in the maintenance of human arm posture," *IEEE transactions on systems, man, and cybernetics,* vol. 23, no. 3, pp. 698-709, 1993.

[3] N. Hogan, "The mechanics of multi-joint posture and movement control," *Biological cybernetics,* vol. 52, no. 5, pp. 315-331, 1985.

[4] E. J. Hegedus, A. P. Goode, C. E. Cook, L. Michener, C. A. Myer, D. M. Myer, and A. A. Wright, "Which physical examination tests provide clinicians with the most value when examining the shoulder? Update of a systematic review with meta-analysis of individual tests," *British journal of sports medicine,* vol. 46, no. 14, pp. 964-978, 2012.

[5] D. B. Lipps, E. M. Baillargeon, D. Ludvig, and E. J. Perreault, "Quantifying the Multidimensional Impedance of the Shoulder During Volitional Contractions," *Annals of Biomedical Engineering*, pp. 1-16, 2020.

[6] T. Tsuji, P. G. Morasso, K. Goto, and K. Ito, "Human hand impedance characteristics during maintained posture," *Biological cybernetics,* vol. 72, no. 6, pp. 475-485, 1995.

[7] E. J. Perreault, R. F. Kirsch, and P. E. Crago, "Multijoint dynamics and postural stability of the human arm," *Experimental brain research,* vol. 157, no. 4, pp. 507-517, 2004.

[8] S. Stroeve, "Impedance characteristics of a neuromusculoskeletal model of the human arm I. Posture control," *Biological cybernetics,* vol. 81, no. 5, pp. 475-494, 1999.

[9] X. Hu, W. M. Murray, and E. J. Perreault, "Muscle short-range stiffness can be used to estimate the endpoint stiffness of the human arm," *Journal of neurophysiology,* vol. 105, no. 4, pp. 1633-1641, 2011.

[10] K. R. Holzbaur, W. M. Murray, and S. L. Delp, "A model of the upper extremity for simulating musculoskeletal surgery and analyzing neuromuscular control," *Annals of biomedical engineering,* vol. 33, no. 6, pp. 829-840, 2005.

[11] K. R. S. Holzbaur, W. M. Murray, G. E. Gold, and S. L. Delp, "Upper limb muscle volumes in adult subjects," *Journal of Biomechanics,* vol. 40, pp. 742-749, 2007.

[12] A. V. Savescu, M. L. Latash, and V. M. Zatsiorsky, "A technique to determine friction at the fingertips," *Journal of applied biomechanics,* vol. 24, no. 1, pp. 43-50, 2008.